Journal of Volcanology and Geothermal Research 402 (2020) 106996

Contents lists available at ScienceDirect

Journal of Volcanology and Geothermal Research

journal homepage: www.elsevier.com/locate/jvolgeores

Examining the statistical relationships between volcanic seismic, infrasound, and electrical signals: A case study of Sakurajima volcano, 2015

Cassandra M. Smith [a,b,*], Glenn Thompson [a], Steven Reader [a], Sonja A. Behnke [c], Stephen R. McNutt [a], Ron Thomas [d], Harald Edens [d]

[a] University of South Florida, Tampa, FL, United States of America
[b] Alaska Volcano Observatory, Anchorage, AK, United States of America
[c] Los Alamos National Lab, Los Alamos, NM, United States of America
[d] New Mexico Institute of Mining and Technology, Socorro, NM, United States of America

ARTICLE INFO

Article history:
Received 14 November 2019
Received in revised form 30 June 2020
Accepted 5 July 2020
Available online 14 July 2020

Keywords:
Volcanic lightning
Continual radio frequency impulses
Multivariable statistics
Logistic regression
Vulcanian eruptions
Explosive volcanism

ABSTRACT

Sakurajima volcano in Japan is known for frequent eruptions containing prolific volcanic lightning. Previous studies from eruptions at Redoubt have shown preliminary correlations between seismic, infrasound, and radio frequency signals. This study uses field data collected at Sakurajima from 28 May–7 June 2015 and multivariable statistical modeling to quantify these relationships. We build regression equations to examine each of the following parameters of electrical activity: (1) the presence of electrical activity, (2) the presence of the radio frequency signal called continual radio frequency impulses (CRF), (3) the presence of lightning, (4) the overall duration of electrical activity, and (5) the total number of radio frequency sources located by a lightning mapping array. We model these response variables against: (1) seismic energy, (2) infrasound energy, (3) seismic duration, (4) infrasound duration, and (5) the volcano acoustic seismic ratio. Our final regression equations show that each parameter of electrical activity is best defined by a separate set of response parameters, but overall events with greater explosivity correlate with higher amounts of electrical activity. Specifically, (1) the probability of CRF occurring, and the overall number of located radio frequency sources are likely related to deeper fragmentation depths; (2) the probability of electrical activity occurring at all, and specifically the probability of lightning being generated are correlated with high infrasound energies indicating that the gas thrust phase of plume formation plays an important role in charge generation; and (3) the longer an eruption (as determined by the duration of the infrasound signal) the longer we can expect to see radio frequency signals generated.

1. Introduction

The high occurrence rate of explosive eruptive activity combined with frequent volcanic lightning makes Sakurajima an ideal volcano for studying the relationship between seismic, infrasound, and radio frequency signals. Sakurajima volcano (Kyushu, Japan) is a stratovolcano that is part of the larger Aira Caldera volcanic complex. Sakurajima is one of the most active volcanoes in Japan, as it has been erupting with intermittent explosive events since 1955, and is well known for its frequent episodes of volcanic lightning (Uhira and Takeo, 1994; Iguchi et al., 2013; Yokoo et al., 2014).

Volcanic lightning can be detected remotely and may give insight into the explosivity of an eruption (Hoblitt, 1994; Thomas et al., 2010; McNutt and Williams, 2010; Arason et al., 2011; Behnke et al., 2014; Shevtsov et al., 2016; Van Eaton et al., 2016; Hargie et al., 2019; Van Eaton et al., 2020). In order to understand what volcanic lightning monitoring may tell us about the source parameters of an explosive eruption it is beneficial to investigate the relationships between parameters measured from seismic, infrasound and lightning data. A possible relationship between the durations of seismic, infrasound, and electrical activity was first noted by Behnke et al. (2013) for explosive activity at Redoubt. However, these relationships have not been analyzed past this initial observation. Seismic and infrasound monitoring are among the most ubiquitous volcanic monitoring methods and they benefit from having been well studied and their signals generally understood for a wide number of eruptive types. However, seismic and infrasound monitoring methods generally require local (<15 km) instrumentation. Furthermore, travel-time delays and signal attenuation may diminish

Abbreviations: CRF, Continual Radio Frequency; LMA, Lightning Mapping Array; NLS, Number of Located Sources; VASR, Volcano Acoustic Seismic Ratio; VHF, Very High Frequency.

* Corresponding author at: University of South Florida, Tampa, FL, United States of America.
E-mail address: cassandramsmith@usgs.gov (C.M. Smith).

https://doi.org/10.1016/j.jvolgeores.2020.106996

the hazard mitigation value of the data if only regional deployments are available. Lightning monitoring is potentially transformative because it can be monitored on local, regional, and global scales with almost no travel time delay because the electromagnetic waves travel at the speed of light (Rakov, 2013). Therefore, by better understanding what volcanic lightning can tell us about the explosive activity we can better use lightning detection instruments to complement existing volcano monitoring capabilities.

This study examines a suite of explosive events from 28 May–7 June 2015. During this time the Showa crater on the eastern flank of the volcano was active. During our 11-day observation period there were tens to hundreds of explosions per day visible as distinct signals in the seismic and infrasound data. The events during this time period included: (1) short lived explosions (<16 s) with clear N-shaped pulses (Morrissey and Chouet, 2010) preceded by a lack of geophysical activity or visible ash venting and, (2) continuous gas and ash emission events that lasted for several minutes to hours distinguishable in the geophysical record by the presence of a sustained infrasonic coda (>30 s to several minutes) and seismic signals that were generally emergent (McNutt et al., 2015).

A lightning mapping array recorded both continual radio frequency (CRF) impulses (Thomas et al., 2007; Behnke et al., 2018) as well as discrete lightning flashes. Just under half of examined events had some form of electrical activity recorded. In this paper we use the term electrical activity as an all-encompassing term for the various types of electrical discharges that volcanoes produce (CRF and volcanic lightning).

This paper gives an in-depth analysis of the statistical relationships between seismic, infrasound, and radio frequency sources. By exploring the underlying statistical relationships between these signals and volcanic electrical activity at Sakurajima, we try to understand what information volcanically generated electrical activity can provide in a monitoring context. A baseline relationship is needed to understand how this electrical activity might vary between different volcanic centers and between eruptions of different scales. Therefore, we examine the following two hypotheses:

1. An increase in explosion size - as defined by the infrasound or seismic energy - will result in more electrical activity in the volcanic plume
2. An increase in the proportion of energy partitioned into the plume - as defined by the volcano acoustic seismic ratio (Johnson and Aster, 2005) - will result in more electrical activity in the volcanic plume.

This paper is organized as follows 1) a brief overview of volcanic seismology, volcanic infrasound, and volcanically generated electrical activity; 2) an explanation of our dataset development for the various geophysical parameters (seismic, infrasound, and lightning); 3) the method for creating the logistic and linear statistical models; and 4) a discussion of the resulting models of volcanic electrical activity and the resulting relationships with seismic and infrasound signals during eruptive events.

2. Background

2.1. Volcanic seismology

Volcanoes produce many different types of seismic signals. Patterns in depth, occurrence rate, and amplitude of these signals usually change prior to volcanic eruptions and escalations in ongoing eruptions (Uhira and Takeo, 1994; Ishihara, 1985). Scientists analyze these patterns in order to monitor and forecast increases in volcanic activity. Once an eruption has begun explosions at the summit transmit energy into the subsurface and these seismic expressions can be used to calculate the strength of eruption (McNutt et al., 2015). It is this relationship between seismic expression and surface processes that we hope to utilize in our examination of volcanic lightning. Examples of seismic (and infrasound) waveforms from Sakurajima can be seen in Fig. 1. Volcanic seismology typically divides signals into the following categories: high frequency or VT (volcanic-tectonic), low frequency, hybrid, tremor, and explosion quakes (McNutt et al., 2015). At Sakurajima the majority of the events that we recorded during our field campaign were explosion quakes and they will be the focus of this paper. Low frequency events and tremor also occurred but because they are not directly related to surface processes, we do not examine them further.

2.2. Volcanic infrasound

The relationships between (1) the energy partitioning of the explosion into the ground versus air, (2) the depth of explosion, and (3) the amount of overburden can be determined through infrasound signals (in combination with seismic signals) (Johnson and Ripepe, 2011), and may be related to electrical activity in the plume. McNutt et al. (2013) noted that there might be an infrasound threshold pressure at which volcanic lightning becomes abundant. The addition of infrasound sensors to a seismic network allows for clear discrimination between subsurface processes (which produce no infrasound) and subaerial/vent-air interface processes, such as explosive eruptions, the destruction of lava plugs, and gas/ash venting that do produce infrasound signals. Infrasound monitoring works on similar principles to seismic monitoring, but with less distortion of the signal as it propagates from source to sensor (Johnson and Ripepe, 2011). During a volcanic explosion, energy is transmitted through both the ground as seismic waves and the atmosphere as infrasound waves. Johnson and Aster (2005) introduced the Volcano Acoustic Seismic Ratio (VASR), which is the ratio of acoustic energy to seismic energy. Johnson and Aster (2005) found that events with larger VASR values corresponded to a variety of

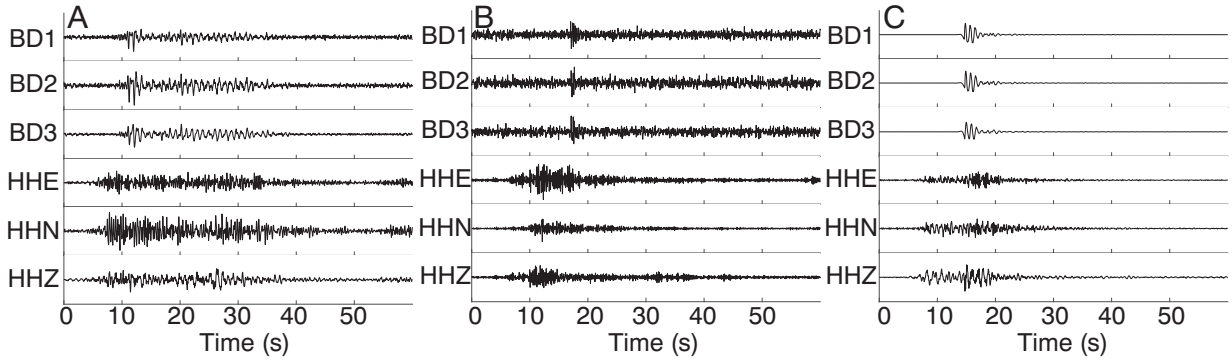

Fig. 1. An example of the different infrasound and seismic waveforms recorded at the SAKA station. In all panels the top three traces are infrasound and the bottom three traces are seismic (E-W, N-S, and vertical respectively). Panel A shows an example of an event where no electrical activity was recorded. Panel B shows an event where electrical activity (such as lightning), but not CRF, was recorded. Panel C shows an event where both electrical activity and CRF were recorded. Vertical scales are normalized between panels.

phenomena including low density plumes, short wide conduits, or a small monopole source region.

Infrasound signals at Sakurajima have been previously studied and noted to include both tremor and impulsive type features as well as 'preceding phases' before lava plug expansion and failure. For a full analysis of the different types of infrasound at Sakurajima we direct the reader to Garcés et al. (1999), Morrissey et al. (2008), and Yokoo et al. (2009).

2.3. Volcanic electrical activity

In this paper we will present data from a lightning mapping array (LMA) system (Rison et al., 1999; Thomas et al., 2003, 2004; Hamlin, 2004). The LMA requires a compact array configuration (<100 km radius), compared to other global lightning detection systems, but allows for highly detailed radio frequency source location measurements. The LMA has been previously used to study electrical activity at Augustine (Thomas et al., 2007; Thomas et al., 2010), Eyjafjallajökull (Behnke et al., 2014; Woodhouse and Behnke, 2014), and Redoubt (Behnke et al., 2013; McNutt et al., 2013; Behnke and Bruning, 2015). LMA data has been used to classify volcanic electrical activity into CRF impulses, near-vent lightning, and plume lightning (Thomas et al., 2007). At remote volcanoes, infrastructure limitations may prevent locally deployed (<15 km) permanent, in-situ seismic and infrasound networks. However, a regional (~100 km radius) LMA system may allow for near-real time monitoring of an explosive eruption through the detection and quantification of volcanic electrical activity. The utilization of LMA data in monitoring arrays would be able to supplement regional seismic and infrasound arrays.

3. Data Collection

3.1. Sensor network

Our field campaign collected a multiparametric suite of data from nine LMA stations, two 3-component Nanometrics Trillium Compact 120-s seismometers, six infraBSU infrasound sensors, and visual observations from 28 May–7 June 2015 (Fig. 2). Due to site access limitations the two seismometers were at similar azimuths (difference of 16 degrees) to the active vent. The distance to each seismometer from the vent was ~3 km (Fig. 2). At each seismic site three infrasound sensors were deployed in a triangular pattern at distances of 22 m from the seismometers. The seismic and infrasound data were recorded on Nanometrics Centaur digitizers at a sample rate of 100 Hz. From our visual observations of the volcano while watching live feeds of the seismic and infrasound recordings we have confidence that the recorded events originated at Showa Crater. Infrasound data were converted from V to Pa using the nominal (manufacturer supplied) calibration of 18 counts/Pa for the infraBSU sensors. The seismometer data were converted using the nominal calibration of 3.33 nm/s per count. The results in this paper will be derived from the LMA and seismic/infrasound data.

In the modeling that follows, for each event the maximum seismic duration and median seismic energy of all six seismic channels was used. Similarly, for each event the maximum infrasound duration and median infrasound energy of all stations was used. Finally, the VASR was calculated by dividing the median infrasound energy by the median vertical seismic energy (Johnson and Aster, 2005). Median values were deemed most appropriate because all sensors were approximately equidistant from the explosion source, and nominal calibrations were assumed. See the Supplemental Materials (A) for a detailed description of event determination. These specific variables were chosen for analysis because combined they give a good summary of the explosive event, are well established in the literature, and are easy to calculate at other volcanoes for future comparison studies (Ishihara, 1985; Uhira and Takeo, 1994; Morrissey et al., 2008; Garcés et al., 1999; Tameguri et al., 2002; Clark et al., 2015; Johnson and Aster, 2005; Yokoo et al., 2009).

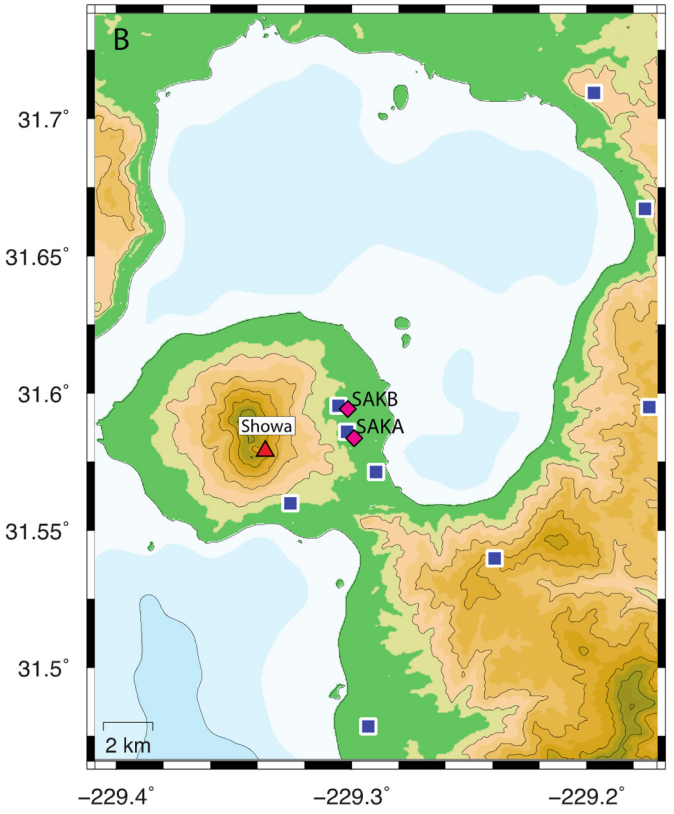

Fig. 2. Sakurajima Volcano instrument map. The red triangle is Showa Crater, located on the southeast flank of the volcano. Pink diamonds, labeled SAKA and SAKB, show the locations of the seismic and infrasound arrays. Blue squares are the locations of the LMA stations. (For interpretation of the references to colour in this figure legend, the reader is referred to the web version of this article.)

3.2. Analysis of electrical activity

A lightning mapping array (LMA) - developed by the New Mexico Institute of Mining and Technology (Rison et al., 1999) - was used to gather detailed lightning data from the eruptions. Due to the increased attenuation of VHF waves over ground, LMA sensors require line-of-sight to the radiation source. Nine LMA stations were deployed at a variety of azimuths (57°–159° from north) and distances (2 km–20 km) from Sakurajima's Showa crater. Showa crater is located on the eastern slope of the volcanic edifice so all of the LMA stations were located on the eastern side of the volcano and bay (Fig. 2).

LMA stations record impulsive very high frequency (VHF) radiation in a 6 MHz passband (for this case we used the 66–72 MHz range), which is emitted during the process of the electrical breakdown of air. The LMA samples at 25 MS/s and records at most one impulse in successive 10 μs windows if the power of the signal exceeds a noise-riding threshold (Behnke et al., 2018). The 3-D locations of impulsive sources are then determined using time-of-arrival (TOA) processing methods.

The parameters derived from the LMA data that are discussed in this paper are (1) the number of located sources (NLS), (2) the duration of electrical activity, and (3) the presence of CRF impulses. The duration of the electrical activity is calculated as the time from the first located source to the last located source within the analyzed window. A typical lightning flash is composed of many (tens to several hundreds or thousands) radio frequency sources (Fig. 3). A located source is determined to be part of a flash or CRF by its location and timing relative to other sources. A flash is defined as three or more sources occurring over a timeframe of 0.1 s with a maximum distance of 100 m between sources.

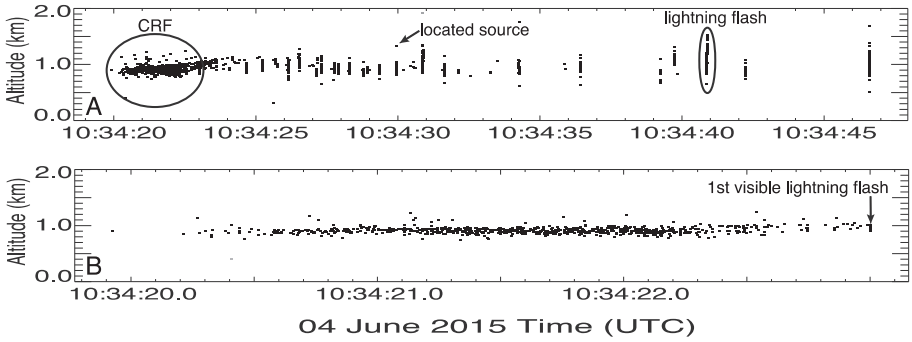

Fig. 3. Example of located LMA data for a single explosive event. Panel A shows labeled examples of CRF, a lightning flash, and a single located radio frequency source. Panel B is a zoomed in view of the circled CRF phase from Panel A. This zoomed in view shows how the end of the CRF phase was determined by manually locating the first visible lightning flash (indicated by the arrow as a vertical alignment of located sources) and classifying all previous activity as CRF.

For this analysis we do not differentiate between near-vent and plume lightning. The CRF phase is visually determined as a high rate of located sources, close to the vent altitude, that occurs nearly continuously (Fig. 3). CRF typically occurs during the active gas thrust phase of an eruption whereas flashes can occur at any point during the eruption, even after active ash venting has stopped and the plume has detached (Behnke et al., 2013; Van Eaton et al., 2016). CRF has been previously related to impulsive, short duration events with seismic amplitudes of >7 μm as recorded at Kurokami, ~3 km from Showa crater (Smith et al., 2018).

4. Statistical analysis

To determine the relationships between volcanic electrical activity and seismic/infrasound data we ran a series of statistical tests using the open source R program and select packages for statistics and graphical outputs (R Core Team, 2017; Fox, 2003; Sarkar, 2008; Fox and Weisberg, 2011; Lumley, 2017). We chose to develop multivariable regressions for these datasets complexity. Explosive volcanic eruptions have a multitude of parameters that may influence the generation of volcanic electrical activity. By using multivariable regressions we are able to take a large suite of variables (in this case 5 predictor variables relating to the seismic and infrasound signals) and determine both (1) which combination of variables is most significant to modeling a specific parameter of electrical activity, and (2) the specific relationships between individual predictor variables and the response variable while holding all other significant variables constant through the use of effect plots. Understanding how volcanic electrical activity is related to individual variables is valuable for this developing field of study.

For our in-depth statistical analyses, we utilized a dual subset method where we broke the overall data set into two subsets based on the presence of electrical activity. Subset 1 was the entire dataset independent of whether there was electrical activity detected or not. Subset 2 contains only those events that had electrical activity. For each subset we ran a statistical analysis of the selected parameter of electrical activity against the seismic and infrasound data. We first looked at Subset 1 and ran a multivariable logistic regression based on the presence or absence of electrical activity. We then ran logistic/linear regressions on Subset 2, based on the following four parameters of electrical activity: (1) presence or absence of CRF, (2) presence or absence of lightning flashes, (3) the total duration of electrical activity, and (4) the total number of located sources. This approach allows us to determine which variables are most relevant to which parameter of electrical activity.

4.1. Model fitting

Some of the variable distributions were skewed and non-normal (Supplemental Materials B). In order to build our models these variables required normalization. The variables were normalized through a variety of transformations including $\log_{10}$ and square-root. To determine the transformation for each variable, we used a combination of (1) visual analysis of histograms and scatterplots and (2) symbox, powerTransform, and the qqPlot functions from the *car* library in R (R Core Team, 2017; Fox, 2003). This set of functions gives suggestions on how to best transform the variable to achieve normality.

An interaction is when the effect of one variable on the response is dependent on the value of another variable. Using initial models, containing all normalized variables, we searched for significant interactions between variables using an iterative process including analysis of variance tests with F-test statistics during model building. Significant interactions are shown in the modeling equations as multiplications.

Stepwise modeling in both forward and backwards directions was then applied to determine the most significant variables to include in each final model. A forward stepwise model starts with none of the explanatory variables included and then determines which of the explanatory variables has the most statistical explanatory power when added to the regression. The model then moves on to the second most explanatory variable and so forth until the model is no longer improved by the addition of new explanatory variables. A backward stepwise model does the reverse, starting with all of the possible explanatory variables and removing the least effective variables, one at a time. For this investigation we used a combination of forward and backward regressions where at each step the model investigated both the addition and deletion of variables. This resulted in our models having the minimum number of variables required to explain the response. For the models presented in this paper, the predictor variables were either statistically significant ($p < 0.05$) and/or were shown to improve the accuracy and stability of the model through stepwise modeling.

4.2. Logistic modeling

Logistic models are members of generalized linear model classes that are used when the response variable is dichotomous – and therefore coded using a binary (value 0 or 1) - to represent an absence or presence of the phenomena in question. For example, lightning was either detected (coded 1) or not (coded 0). The logistic model uses the logit equation (Fox, 2016) to create a model of the mathematical probability of the event in question occurring in the form of an odds ratio which can be easily translated to a probability equation. In this work we use the logistic model to investigate: (1) the overall presence of electrical activity, (2) the presence of CRF, and (3) the presence of lightning flashes.

4.3. Multivariable linear modeling

A multivariable linear model follows the same idea as a traditional linear model except instead of a single predictor variable there are

multiple predictors regressed against a single continuous response variable. In this work we will use the linear model for: (1) the duration of electrical activity, and (2) the number of located radio frequency sources. These values were chosen for linear modeling because they are all continuous variables that may be useful in a monitoring context in quantifying the electrical activity.

4.4. Effect plots

Multivariable models cannot be presented as single, simple 2-D plots with a regression line. Therefore, in this paper we will rely on effect plots to show the model results. An effect plot is generated by the predicted values of the response variable (the parameter of electrical activity) on the y-axis for a range of one of the predictor variables (the seismic or infrasound related parameter) shown on the x-axis. For these plots the rest of the variables included in the model are held at a constant value (their mean value) so that the effect of the single predictor on the response can be visualized. In models that include interactions, the effect plots use multiple panels to show the effect of different levels of one explanatory variable across a range of the second explanatory variable on the response variable. These are shown in modeling subsets Sub2.Mod3 and Sub2.Mod4 below. The statistical terminology for how the predictor and response variables relate on these plots is the 'effect' of the predictor on the response – this is a statistical term and does not imply a cause-and-effect relationship in the physical world.

4.5. Statistical parameters

The R-squared and Macmillan's pseudo R-squared are statistics that describe the percentage of the variation in the model that can be described by the model's predictor variables. Macmillan's pseudo R-squared is calculated by subtracting the ratio of the residual deviance to the null deviance from 1. The R-squared and pseudo R-squared values for these models range from 0.04–0.35. Although these values are relatively low, they are expected due to the high number of unknowns that we cannot account for in these models. Volcanic systems are highly complex and many other parameters may play a role in the production of electrical activity, including variables such as ascent rate, gas content, and plume dynamics (Behnke and McNutt, 2014; McNutt and Williams, 2010; James et al., 2008). Specifically, the relationships between exploded material and plume/atmospheric properties will influence charging mechanisms (Méndez Harper et al., 2018; Nicoll et al., 2019; Stern et al., 2019; Prata et al., 2020; Van Eaton et al., 2020). However, for this analysis we are focused on the potential relationships between the explosive event and volcanic electrical activity in order to determine if monitoring volcanic electrical activity will be useful in understanding the scale of the explosive event.

Other statistical parameters used to determine the quality of our models include standard errors, t-values or z-values (for linear and logistic models respectively), and *p*-values. The standard error is the square root of the variance of a statistic. In this paper, the standard error listed is for the standard error on the slope coefficient (β). The t-value (or its logistic model equivalent of the z-value) is used to test the null hypothesis that $\beta = 0$. The p-value gives the probability that the t-value will fall outside of the designated confidence interval (typically given at 95% for statistical significance). A significant p-value (<0.05) indicates that the null hypotheses can be rejected. These statistics are used to determine the confidence intervals of the models, which are shown as shaded areas on the effect plots.

5. Results and discussion

This section will first outline some overall trends seen in the catalog. Then each of the five regression models will be presented and subsequently discussed one-by-one. This section will end with a summary discussion of all models.

5.1. Catalog trends

Our catalog contained 2778 detected events (Table 1). Of these, 1478 events had both seismic and infrasound signals. The remaining 1300 events lacked either seismic or infrasound signals.

Table 1 shows a daily tabulation of explosive events, including both seismic and infrasound data, for the observation period of 28 May–7 June 2015. The period of 5 June–7 June UTC was the most active period with ~800 events recorded. CRF was recorded in 4.1% of events, 36.3% of events had no CRF but did have other electrical activity, and the remaining 59.6% of eruptive events had no electrical activity at all.

Fig. 4 gives a visual overview of the catalog with respect to the seismic and infrasound energies as well as the recorded electrical activity. This plot is in the style of the Volcano Acoustic Seismic Ratio (VASR) plots for Johnson and Aster (2005). Seismic energies (J) ranged from ~10^2–~10^9 J. Infrasound energies ranged from ~10^3–~$10^{9.5}$ J. The data cluster into 3 distinct groups. Cluster A shows the group of events that have a high VASR but no radio frequency signal. Cluster B has a similar range of VASR to Cluster A, but contains the highest recorded infrasound energies and also high levels of electrical activity – including CRF, lightning, and high NLS counts. Cluster C is similar to Cluster A in infrasound energies but with slightly higher seismic energies and thus consists of lower overall VASR values than Cluster A. This may be related to events in Cluster C having more ash in the plume. Gaudin et al. (2018) and Gaudin and Cimarelli (2019) have shown experimentally that the presence of ash is a requirement for electrical discharges in the plume. A greater presence of ash (charge carriers) would enhance lightning while at the same time attenuating the infrasound; therefore, the resulting event would have a low VASR value. The lack of radio frequency signals in Cluster A may indicate that these events had low ash content and were more gaseous plumes.

5.2. Subset 1 model 1 (Sub1.Mod1) logistic model with respect to electrical activity

The first step of our statistical analysis of the data was to organize it via a 2-factor division of whether there was electrical activity or not. For this portion of the analysis we did not differentiate between CRF and volcanic lightning.

5.2.1. Modeling result

We ran a logistic regression on this dataset using the factor of yes/no for electrical activity as our response variable. The final model's regression equation is as follows:

Table 1
Daily electrical activity, 28 May–7 June 2015.

Date (UTC)	Events containing electrical activity and CRF	Events containing electrical activity but not CRF	Events containing no electrical activity	Total events for day
28-May	0	3	0	3
29-May	6	35	29	70
30-May	3	9	115	127
31-May	7	33	58	98
1-Jun	0	13	45	58
2-Jun	7	30	49	86
3-Jun	3	99	81	183
4-Jun	7	27	22	56
5-Jun	17	126	88	231
6-Jun	2	50	266	318
7-Jun	9	111	128	248
Total	61	536	881	1478

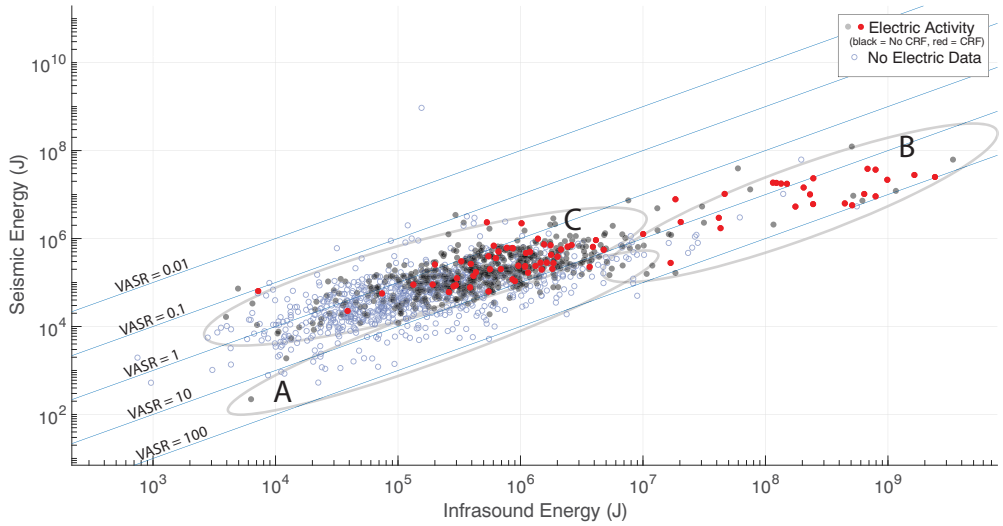

Fig. 4. VASR style plot showing distinct clusters of electrical activity. Blue dots correspond to events that did not have any electrical activity. Black dots correspond to events that had electrical activity but no CRF (see Table 3.1 for numerical breakdown). Red dots correspond to events that had electrical activity including CRF. Three clusters of points are shown, designated A, B, and C. These Clusters are purely qualitative and chosen based on visual examination of the data. Cluster A shows the region where the majority of recorded events had no electrical activity. Cluster B shows the region where the majority of recoded events had electrical activity, including CRF recorded. Cluster C shows the region where there is a gradational change as the infrasound increases from events without electrical activity to events with electrical activity. (For interpretation of the references to colour in this figure legend, the reader is referred to the web version of this article.)

$$Probability\ of\ Electrical\ Event = \frac{1}{1 + \exp\left(-\left(\beta_0 + \beta_V \log_{10} VASR + \beta_{IE} \log_{10} IE + \beta_{ID} \sqrt[2]{ID} + \beta_{SD} \sqrt[2]{SD}\right)\right)} \quad (1)$$

where β is the Beta Coefficient and the corresponding subscripts and variables include IE for infrasound energy, SD for seismic duration, ID for infrasound duration, and VASR for the Volcano Acoustic Seismic Ratio. Beta coefficients and statistical parameters are given in Table 2. The effect plots for this model are given in Fig. 5.

This model demonstrates significant relationships between the presence of electrical activity and four of the five chosen explanatory variables. Out of this set of variables the relationship between electrical activity and the VASR is quite interesting. As the VASR increases, there is a significant decrease in the probability of electrical activity occurring (Fig. 5A). This initially seems in contradiction with the relationship shown in Fig. 5B where as the infrasound energy increases the probability of electrical activity also increases. Surprisingly, the effect plots of the seismic and infrasound duration also show opposite effects on the probability of the occurrence of electrical activity. An increase in the duration of the seismic signal (Fig. 5C) and a decrease in the duration of the infrasound (Fig. 5D) are both related to higher probabilities of electrical activity.

5.2.2. Model discussion

By examining the effect size (change in probability based on the change in the given variable) and polarity (direction of change) of the effect plots (Fig. 5), we can see that overall this model indicates that the probability of electrical activity increases the most with larger explosions (as indicated by high infrasound energy). The other variables in the model are related to the duration of signals and the relative partitioning of the energy, which may be due to variations in properties such as magma plug development or plume densities. Henceforth, we will discuss each of these possibilities.

5.2.2.1. Magma plug development. This model suggests that high-energy, short duration infrasound signals result in a higher probability of volcanic electrical activity. These signal characteristics have been related to the destruction of a magma plug, resulting in an open conduit system. Our infrasound signals are similar to those described by Yokoo et al. (2009) who showed that Vulcanian eruptions - related to the destruction of a magma plug in the conduit - displayed N-shaped infrasound signals with a small but increasing preceding phase. Our seismic signals are also similar to those described by Tameguri et al. (2002) in their in-depth discussion on explosive seismic signals at Sakurajima, where they also described a fractured lava-dome capped conduit as the cause of the signals.

Additionally, if a magma plug had either not yet developed, or a weakness in the magma plug had allowed partial fracturing and localized permeable degassing, there may not have been enough of a pressure build up to fragment juvenile magma into ash. An examination of the inter-event times shows a small but statistically significant ($p = 0.029$, Supplemental Materials C) difference between events with electrical activity and events without. Events with electrical activity average longer inter-event times by an average of approximately 5 min. With more time between successive eruptions a more substantial plug can solidify, allowing for higher pressures to build up before the explosion.

This interpretation is further enhanced by our field observations. While observing the volcano we noted that prior to the visually largest explosive eruptions there would be a pause in activity of a couple hours, followed by the cessation of fumarole activity in the vent. One possibility to explain the visual cessation of the fumaroles prior to highly explosive events is that that the magma plug had reduced permeability, and the subsequent possible build-up of any exsolved gases, might have preceded each of the larger eruptions.

As infrasound energy increases and infrasound duration decreases, the probability of electrical activity in the plume increased (Fig. 5B, D). The events with high infrasound energy (>10^7 J) also had higher VASR

Table 2
Sub1.Mod1 logistic model with respect to electrical activity.

	Beta coefficient (β)	Standard error	z-Value
Intercept	−9.864	0.665	−14.828***
Infrasound energy (IE)	1.608	0.133	12.133***
Seismic duration (SD)	0.519	0.154	3.359***
Infrasound duration (ID)	−0.372	0.139	−2.672**
VASR	−1.365	0.173	−7.891***
Macmillan's pseudo R^2	0.17		

*>95%, **>99%, ***>99.9% significance level

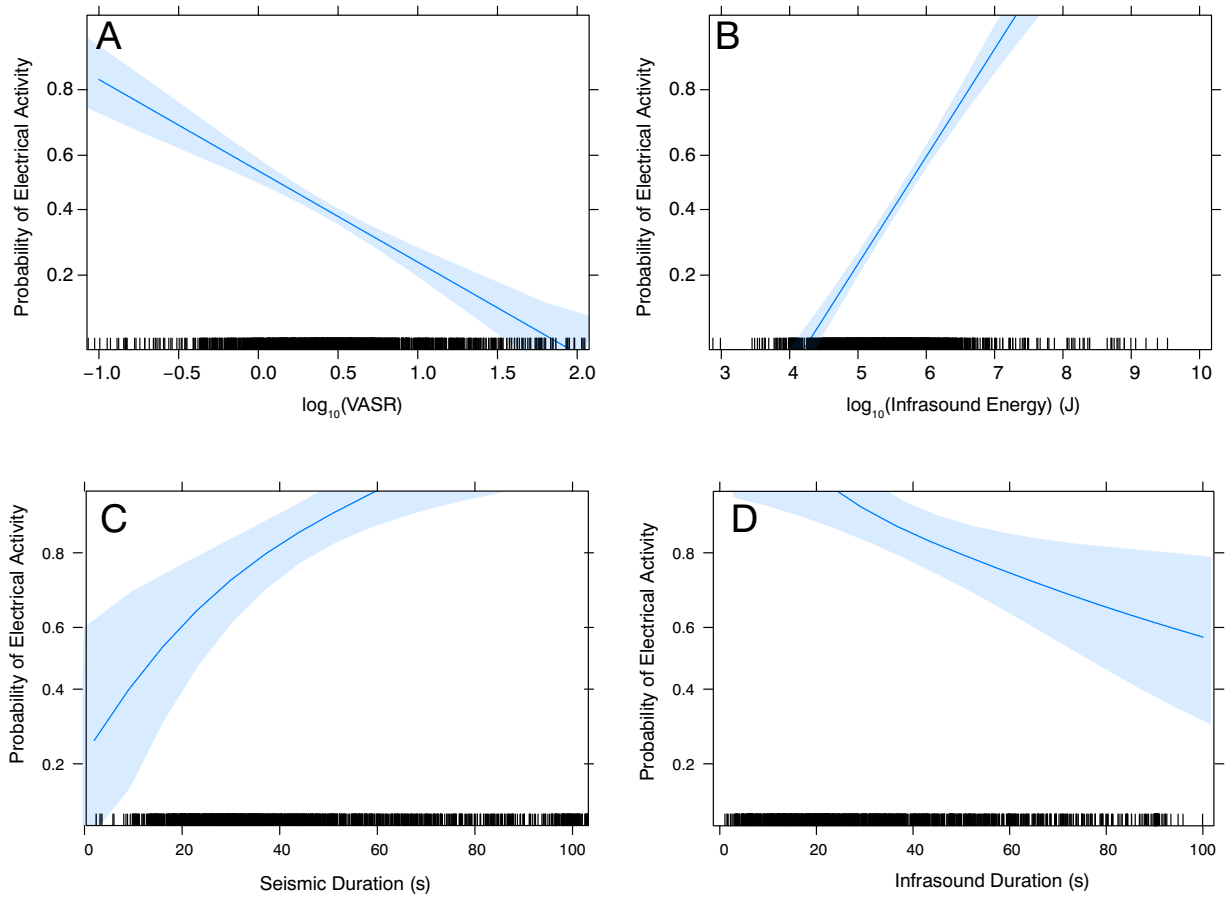

Fig. 5. Statistical effect plots for Sub1.Mod1 logistic model with respect to electrical activity. Panel A shows the negative effect of increasing the VASR on the probability of electrical activity occurring. Panel B shows the positive effect of increasing infrasound energy on the probability of electrical activity occurring. Panel C shows the positive effect of increasing the seismic duration on the probability of electrical activity occurring. Panel D shows the negative effect of increasing the infrasound duration on the probability of electrical activity occurring. Refer back to Section 4.4 for explanation of the structure of these plots.

values (>~5, Fig. 4 Cluster B). Johnson and Aster (2005) relate high VASR values to wide and open conduits, with long-duration, low-amplitude seismic signals as more energy is emitted as infrasound. This is consistent with seismic energy not being significant to the model (and therefore not included) but seismic duration being significant (Fig. 5C). Therefore, using the infrasound, seismic, and VASR information we can speculate that there is a relationship between the destruction of a magma plug, resulting in an open conduit, and the production of volcanic electrical activity.

5.2.2.2. Plume ash content. Fig. 4 suggests that there is a threshold value (~10^7J) for the infrasound energy above which electrical activity is almost certain to occur in the plume. This is reflected in infrasound being one of the significant variables of Sub1.Mod1. This infrasound threshold in conjunction with the Macmillan's pseudo-R^2 of 0.17 indicates that there may be other factors at play not accounted for in this model, such as, the ash content of the plume. Morrissey et al. (1998) suggest that a high-density (high proportion of ash) plume may result in a lower than expected infrasound energy value due to the infrasound energy being expended in the process of evacuating the conduit of ballistics and ash. Therefore, less of the energy travels away from the immediate vent to be recorded. Johnson and Aster (2005) quantified this relationship using mass-dependent transfer of explosive energy into acoustic energy with respect to volumetric acceleration and demonstrated that the addition of solid material into a plume may change the infrasound signal by up to two orders of magnitude. The infrasound signal of an otherwise large explosion may be attenuated by the ash and ballistic content of the plume. Because the infrasound energy may be affected by the plume density, multivariable models are vital to determine which other parameters (e.g. signal durations or VASR) are indicative of the presence of electrical activity.

5.3. Subset 2: events with measured electrical activity

Our second subset of statistical analysis was focused on only those events that had measured electrical activity. We developed four statistical models (Sub2.Mod1 – Sub2.Mod4), one for each investigated parameter of electrical activity (CRF, lightning, the duration of electrical activity, and NLS).

5.3.1. Sub2.Mod1 - logistic model with respect to CRF

5.3.1.1. Modeling result. For our investigation into CRF we used the presence or absence of a CRF signal as our response variable. The final model's regression equation is as follows:

$$\textit{Probability of CRF} = \frac{1}{1 + \exp(-(\beta_0 + \beta_V \log_{10} VASR + \beta_{SE} \log_{10} SE))} \quad (2)$$

where β is the Beta Coefficient and the corresponding subscripts and variables include SE for seismic energy, and VASR is as above. Beta coefficients and statistical parameters are given in Table 3. The effect plots for this model are given in Fig. 6.

The effect plots show that the increase in seismic energy has a much greater effect (greater change on the y-axis) on the probability of CRF than the increase in the VASR value.

Table 3
Sub2.Mod1 logistic model with respect to CRF.

	Beta coefficient (β)	Standard error	z-Value
Intercept	−10.390	1.198	−8.676***
Seismic energy (SE)	1.432	0.212	6.752***
VASR	0.680	0.276	2.466*
Macmillan's pseudo R^2	0.17		

*>95%, **>99%, ***>99.9% significance level

5.3.1.2. Model discussion. The logistic model for the presence of CRF shows a significant positive relationship with the seismic energy and the VASR calculation. The VASR relationship has a smaller overall effect than the seismic signal. This indicates that in order to generate CRF there needs to be a large explosion (indicated here by the large seismic energy) (Smith et al., 2018). We can speculate that the large seismic response may indicate more magma fragmentation in the conduit, which in turn would lead to more juvenile ash (charge carriers) traveling up and out of the conduit. A high proportion of juvenile ash at Sakurajima has been previously related to both the presence of CRF and high amplitude (>7 μm) seismic signals (Smith et al., 2018).

The probability of CRF is further enhanced when a greater proportion of the released energy is emitted as infrasound (shown here as an increasing VASR value). An examination of the difference in arrival times between P-waves and the ground-coupled airwave on the vertical seismic channel indicates that larger VASR values may be related to shallower explosion depths (Supplemental Materials D). Additionally, recent work done by Méndez Harper et al. (2018) shows how small electrical discharges produced in the lab are associated with an overpressurization of the volcanic flow at the vent (likely resulting in high VASR values) and only exist, experimentally, while this overpressurization is maintained. The smaller effect size of the VASR in comparison to the seismic energy may be explained by the density of the plume. Higher density plumes result in lower overall VASR values (Johnson and Aster, 2005). This may cause lower than expected VASR values for the given seismic energies and result in a smaller effect within the model.

5.3.2. Sub2.Mod2 - logistic model with respect to lightning

5.3.2.1. Modeling result. For this model we divided the events that contained radio frequency signals into two sets depending on whether or not there were lightning flashes. This yes/no was used as our response variable. The final model's regression equation is as follows:

$$\textit{Probability of Lightning} = \frac{1}{1 + \exp\left(-\left(\beta_0 + \beta_{IE}\,\log_{10} IE + \beta_{ID}\sqrt[2]{ID}\right)\right)} \quad (3)$$

where β is the Beta Coefficient and the corresponding subscripts and variables are as above. Beta coefficients and statistical parameters are given in Table 4. The effect plots for this model are given in Fig. 7.

For this statistical model, the effect plots show that the presence of lightning flashes in the plume is significantly related to the energy and duration of the infrasound signal, but not the seismic signal. Fig. 7 shows that an increase in both the infrasound energy and the infrasound duration are related to an increase in the probability of lightning occurring. From examining the probability axis of these effect plots

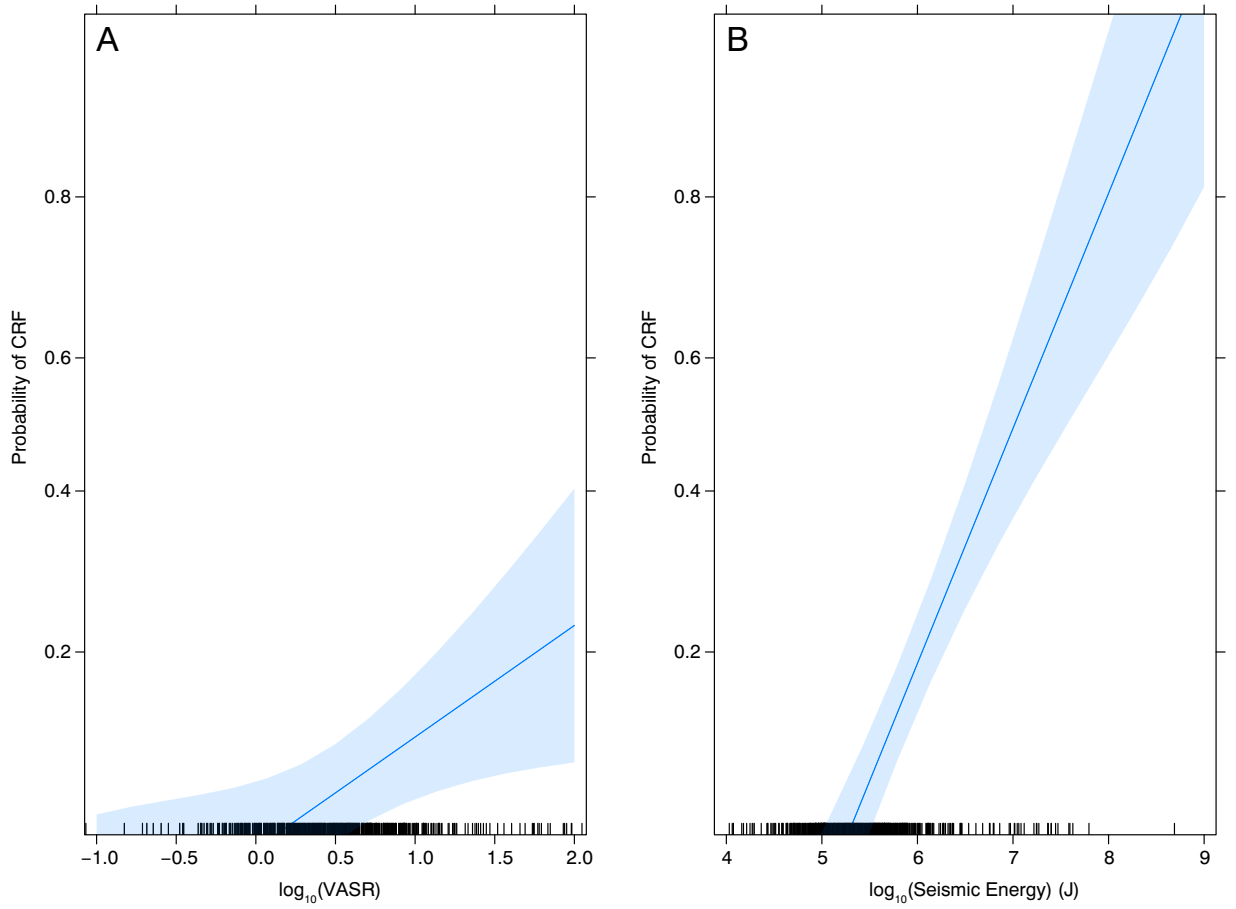

Fig. 6. Statistical effect plots for Sub2.Mod1 logistic model with respect to CRF. Panel A shows the positive effect of increasing the VASR on the probability of CRF occurring. Panel B shows the positive effect of increasing the seismic energy on the probability of CRF occurring. Refer back to Section 4.4 for explanation of the structure of these plots.

Table 4
Sub2.Mod2 logistic model with respect to lightning flashes.

	Beta coefficient (β)	Standard error	z-value
Intercept	−2.585	0.775	−3.336***
Infrasound energy (IE)	0.507	0.147	3.457***
Infrasound duration (ID)	0.100	0.049	2.034*
Macmillan's pseudo R^2	0.04		

*>95%, **>99%, ***>99.9% significance level

we can determine that the size of the effect of the infrasound energy is ~2.5 times larger (spanning a range of probabilities from 0.5–1) than the effect size of the duration of the infrasound (spanning a range of probabilities from 0.8–1).

5.3.2.2. Model discussion. The logistic model with respect to the presence of lightning flashes shows that lightning is positively correlated with the energy and duration of the infrasound signal. To examine the model for multicollinearity (where relationships between variables may cause model instability) we examined the direct relationship between infrasound energy and infrasound duration. Fortunately - with an R^2 of 0.16 for events in subset 2 and an R^2 of 0.24 for all events in subset 1 - the infrasound energy and duration are not directly correlated to each other. The final model has a variance inflation factor (vif) of only 1.17, which is well below the threshold (typically chosen as 4) where correlation between explanatory variables may be considered a problem within the model. Therefore, this model can be considered stable even with only infrasound derived explanatory variables.

The model's effect size of the probability with respect to infrasound duration is positive but small (Fig. 7). The effect size in relation to the infrasound energy is much larger. The correlation between long duration events and lightning suggests that an extended duration of energy input enhances the production of lightning. The high-energy input for an extended duration would directly impact charging mechanisms in the plume by prolonging the gas thrust phase of the eruption (Marchetti et al., 2009). An extended gas thrust phase may indicate that deeper levels of fragmentation may have occurred, which would provide more charged material to the plume (Cashman and Scheu, 2015). An extended gas thrust phase has been shown to promote the charge generation and separation required for the development of lightning, especially the small near-vent flashes that are common at Sakurajima (Cimarelli et al., 2016). This model suggests that the presence or absence of lightning flashes can be statistically predicted by infrasound parameters that indicate an extended gas thrust phase, possibly as the result of increased gas pressure and a larger volume of gas building up prior to the explosive event, resulting in charge generation within the plume.

5.3.3. Sub2.Mod3 - linear model with respect to duration of electrical activity

5.3.3.1. Modeling result. The overall duration of electrical activity is calculated by the time elapsed from the first located radio frequency source to the last located radio frequency source associated with a particular explosive eruption. The final model's regression equation is as follows:

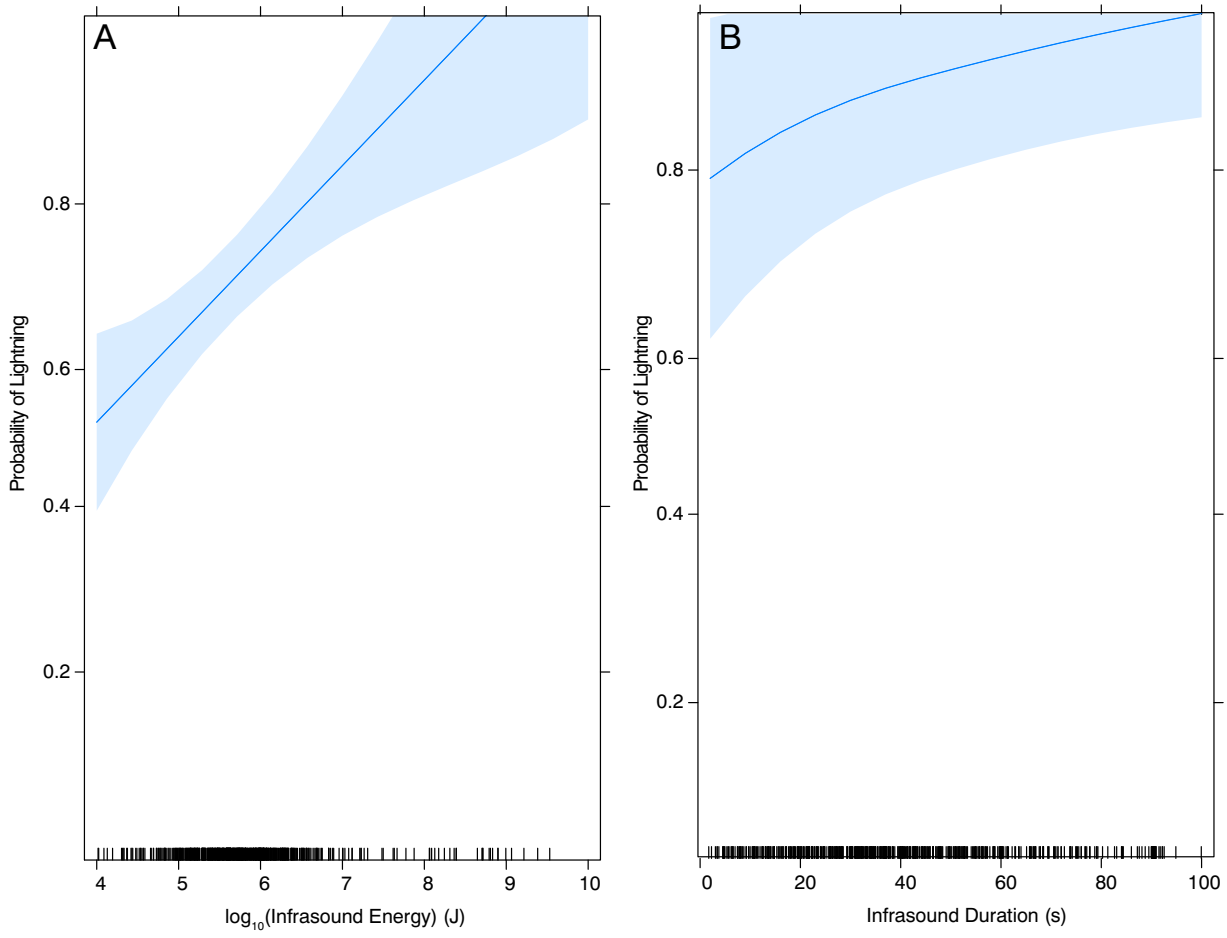

Fig. 7. Statistical effect plots for Sub2.Mod2 logistic model with respect to lightning flashes. Panel A shows the positive effect of increasing the infrasound energy on the probability of lightning occurring. Panel B shows the positive effect of increasing the infrasound duration on the probability of lightning occurring. Refer back to Section 4.4 for explanation of the structure of these plots.

Table 5
Sub2.Mod3 linear model with respect to the duration of electrical activity.

	Beta coefficient (β)	Standard error	t-Value
Intercept	11.086	3.689	3.005**
Seismic energy (SE)	−1.700	0.709	−2.397*
Infrasound duration (ID)	−1.683	0.520	−3.238**
Interaction between Seismic energy and infrasound duration (X1)	0.353	0.097	3.652***
R^2 value	0.08		

*>95%, **>99%, ***>99.9% significance level

$$\sqrt[2]{EA} = \beta_0 + \beta_{SE}(\log_{10}SE) + \beta_{ID}\left(\sqrt[2]{ID}\right) + \beta_{X1}\left(\log_{10}SE * \sqrt[2]{ID}\right) \quad (4)$$

where β is the Beta Coefficient and the corresponding subscripts and variables include X1 for the interaction term and remaining variables are as above. Beta coefficients and statistical parameters are given in Table 5. The effect plots for this model are given in Fig. 8.

The model shows that the duration of electrical activity is significantly correlated to the interaction between seismic energy and the duration of infrasound signal. As shown in Fig. 8, as the infrasound duration increases, the effect of the seismic signal on the duration of electrical activity switches from a negative coefficient at low infrasound durations to a strongly positive coefficient at higher infrasound durations.

5.3.3.2. Model discussion. The linear model relating to the duration of the electrical activity shows that the interaction between the seismic energy and the infrasound duration variable has a significant effect on the duration of the electrical activity. Assuming that the infrasound duration is equivalent to the duration of the explosive event, for short duration explosive events (1–16 s, Panel A and B, Fig. 8), as the seismic energy increases, the duration of the electrical activity generally decreases (the increase at the high end of the seismic energy in Panel A is likely due to the large error range due to a small amount of data in this region). This type of event is likely a deeper seismic event with a small gaseous, ash-poor plume forming at the surface. When the infrasound duration is increased (36 s–100 s) across the same scale of seismic energies (Panel C–E, Fig. 8) the trend is inverted, with the duration of electrical activity increasing as the seismic energy increases. This indicates an explosive event where the explosion source is possibly either (1) closer to the surface so that infrasound is emitted at the vent for a longer period of time (this may explain the low seismic energy/long duration events) or (2) an event that releases more seismic energy resulting in a longer infrasound signal as more energy is released (this may explain the high seismic energy/long infrasound duration events).

From field observations, this increase in the duration of the infrasound signal appears to correspond to an increase in the duration of ash venting. An increase in the ash venting duration would allow for an increase in overall charging through ash interaction methods such as triboelectric charging and fracto-emission (Méndez Harper and Dufek, 2016). As particles are charged for longer periods of time, the duration of the resulting electrical activity would also increase, and there would be a higher net charge in the plume. Future research using a seismo-acoustic array with more stations and better azimuthal

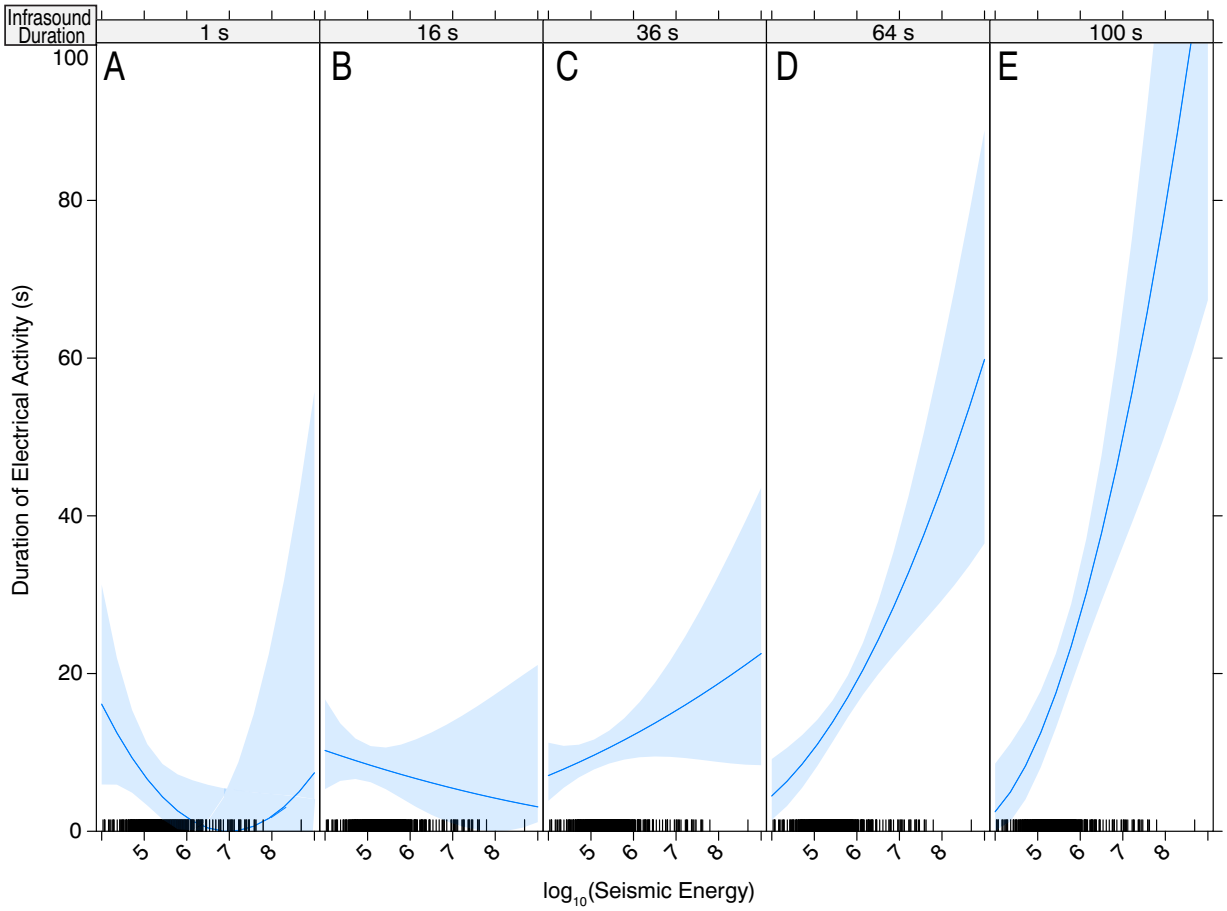

Fig. 8. Statistical effect plots for Sub2.Mod3 linear model with respect to duration of electrical activity. Panel A and B show the negative effect of increasing seismic energy (at short infrasound durations and lower seismic energies) on the overall duration of the electrical activity. Panels C-E show the positive effect of increasing seismic energy (at mid to long infrasound durations) on the overall duration of electrical activity. Refer back to Section 4.4 for explanation of the structure of these plots.

Table 6
Sub2.Mod4 linear model with respect to NLS.

	Beta coefficient (β)	Standard error	t-Value
Intercept	94.428	15.416	6.125***
Seismic energy (SE)	−19.539	2.835	−6.893***
Infrasound energy (IE)	−16.998	2.561	−6.638***
Interaction between seismic energy and infrasound energy (X2)	3.587	0.412	8.705***
Seismic Duration (SD)	0.367	0.227	1.618
R^2 value	0.35		

*>95%, **>99%, ***>99.9% significance level

coverage, and therefore the ability to determine the detailed 3D locations of these explosive events in the conduit, will greatly improve the interpretations of this model.

5.3.4. Sub2.Mod4 – linear model with respect to number of located sources

5.3.4.1. Modeling result. The number of located sources (NLS) is a total measure of the VHF sources that were located by the LMA. This count does not differentiate between CRF and lightning flashes but instead is a value that represents the overall amount of electrical activity of the plume. The final model's regression equation is as follows:

$$\sqrt[2]{NLS} = \beta_0 + \beta_{SE}(\log_{10}SE) + \beta_{IE}(\log_{10}IE) + \beta_{X2}(\log_{10}SE * \log_{10}IE) + \beta_{SD}\sqrt[2]{SD} \quad (5)$$

where β is the Beta Coefficient and the corresponding subscripts and variables include X2 for the interaction term and other variables are as above. Beta coefficients and statistical parameters are given in Table 6. The effect plots for this model - (i) the interaction between the seismic energy and the infrasound energy and (ii) the seismic signal duration - are given in Fig. 9.

The model shows that at low infrasound energy the NLS remains relatively constant (within the confidence intervals) across the range of seismic energy values. However, at larger infrasound energy values the NLS generally increases across the range of seismic energies. However, at the high infrasound energy and low seismic energy range (initial part of panel E) the NLS initially seems to decrease before rapidly increasing with increasing seismic energy. This is likely due to the lack of data points in this range, which leads to larger uncertainties in the model. As shown in panel F the NLS increases non-significantly (p-value >.05) with an increase in the seismic duration.

5.3.4.2. Model discussion. To interpret the linear model for the number of located sources (NLS) described in Eq. (5) it is helpful to consider seismic vs. infrasound energy partitioning and what it may mean for plume development. When there is low infrasound energy (see panel A, B of Fig. 9), as seismic energy increases, the predicted NLS stays close to constant, with a potential small increase at the high end of Panel A (within confidence interval). This indicates that when there is a higher proportion of seismic to infrasound energy there will be less resulting electrical activity, regardless of the strength of the seismic event. This may result from the explosion event occurring at a deeper source point so that most of its energy is propagated as seismic waves and very little energy reaches the surface as infrasound (Uhira and Takeo, 1994, Supplemental Materials D). A deep event with little surface expression would likely have a small plume with little turbulence or ash. This would negatively affect the occurrence of electrical activity.

As infrasound energy increases (moving from panel A to E in Fig. 9) the overall proportion of infrasound to seismic energy increases. In panels C-E a threshold has been crossed where the proportion of infrasound to seismic energy results in a clear increase in the NLS as the seismic energy increases. This may indicate that in order to have a high NLS (high overall electrical activity in the plume), there needs to be a large explosive event that is near the surface, resulting in high infrasound partitioning into the air. If we refer back to Fig. 4 we can see that this threshold of 10^7 J in infrasound energy is observed as the dividing region between Cluster A and Cluster B, where events with electrical activity become prominent.

The inclusion of the seismic duration in the model may indicate a deeper fragmentation depth, which may be significant for ash generation. Following the Vulcanian explosion model in Clarke et al. (2015) Vulcanian explosions occur as a decompression wave and a fragmentation wave that travel from the fractured magma plug down into the conduit, decompressing and fragmenting the magma. For this dataset, where each seismic signal corresponds to an explosive event, a longer duration seismic signal may suggest that the fragmentation wave has travelled deeper into the conduit due to favorable conditions (Clarke

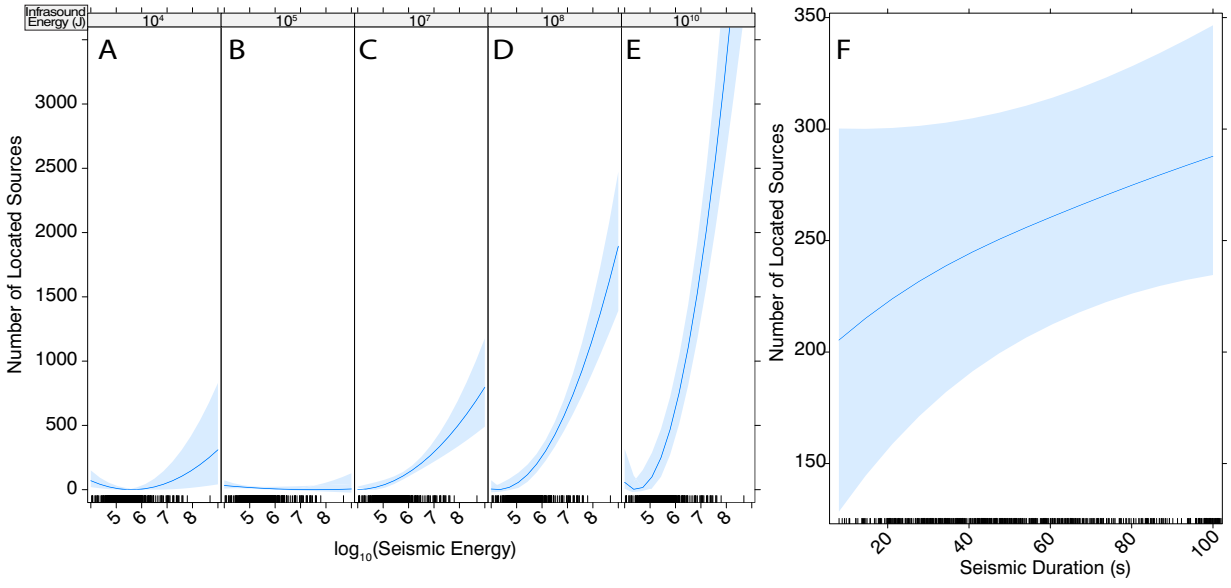

Fig. 9. Effect plots for Sub2.Mod4 linear model with respect to the number of located sources (NLS). Panels A-E show the neutral to positive effect of increasing seismic energy (at mid to large infrasound energies) on the overall NLS. Panel F shows the non-significant (p-value >.05) positive relationship between increasing the seismic duration and increasing the overall NLS. Refer back to Section 4.4 for explanation of the structure of these plots.

et al., 2015). This would imply that more juvenile (deeper) magma is fragmented and travels for a longer distance within the conduit interacting with both the conduit walls and other ash particles – indicators of more electrical activity as suggested in Smith et al. (2018). Alternatively, the explosion duration variation could be explained by the explosion process taking place over a longer period of time, in a single location. However, for this analysis we will use the assumption that longer duration events correspond to the fragmentation wave reaching deeper depths.

5.4. Overall discussion of regression modeling

Our initial hypotheses for this study were that (1) large explosive eruptions, and (2) eruptions where a majority of the energy was partitioned as infrasound, would result in higher levels of electrical activity in the volcanic plume. Through our five regression models (detailed above) we have been able to show evidence for those two general hypotheses and speculate on how individual types of electrical activity are related to physical processes at the vent. Specifically, the relationship between larger explosive events and higher probabilities of, or quantitatively more, electrical activity is clearly shown in Subset 2 Model 1 (Sub2.Mod1) where an increase in seismic energy is decisively correlated with an increase in the probability of CRF occurring. The hypothesized relationship between greater infrasound partitioning and overall electrical activity is also found to be valid. Although Sub1. Mod1 shows that an increasing VASR relates to a decreasing probability of overall electrical activity, this can be explained through the relationships shown in Fig. 4 (where high VASR events that do not have any electrical activity occur at low seismic and low acoustic energies), and through possible interactions with other unmeasured variables, such as plume density. Model Sub2.Mod1 specifically shows that higher VASR values are related to higher probabilities of CRF production. In general, all models suggest that highly explosive events with relatively long gas thrust phases will result in higher levels of electrical activity, regardless of the specific type of electrical activity examined.

See Supplemental Materials (E) for a sensitivity analysis of these models with respect to possible uncertainties in LMA data.

6. Conclusions

Our initial hypotheses were that relatively large explosive events (as defined by seismic or infrasound energy) that had a high proportion of infrasound energy (as defined by the VASR) would result in higher quantified electrical activity. What we found, for Sakurajima, aligns with the first hypothesis, with high infrasound energy being of particular importance to electrical activity, but also shows the complicated and sometimes non-intuitive relationships between electrical activity and geophysical parameters (Eqs. (1)–(5)). For example, in slight contrast to our second hypothesis the probability of electrical activity is negatively correlated to VASR (Eq. (1)). This is further exemplified by each parameter of electrical activity having a different set of significant predictor variables and different relationships between predictors (linear and interaction terms). In summary:

1) The probability of electrical activity occurring is positively correlated with high ($>10^7$J) infrasound energies, which may be related to the development and subsequent fracturing/destruction of a magma plug. The negative correlation of VASR with the probability of electrical activity may indicate that high density, ash rich plumes (low VASR) are more likely to generate electrical activity.
2) The probability of CRF generation is positively correlated with increasing seismic energy, which we interpret as indicating deeper/more magma fragmentation. This also implies a longer duration of particle-particle collisions as they travel out of the conduit – allowing for more triboelectrification.
3) The probability of lightning generation is positively correlated with increasing infrasound energy and duration, indicating that the duration and strength of the plume's gas thrust phases are important for lightning generation.
4) The overall duration of electrical activity is related to the interaction between seismic energy and infrasound duration. We interpret this to be related to plume dynamics where an increase in the duration of ash venting enhances the duration of electrical activity.
5) The overall number of radio frequency sources recorded is related to the interaction between the seismic and infrasound energies, and the seismic duration. We interpret this to indicate that deeper magmatic fragmentation levels result in an increase in overall electrical activity, possibly because of increased ash interactions in the conduit.

Threading through all five models we see that the general trend is that larger explosions (measured by seismic energy or infrasound energy) correlate with increased electrical activity (measured by higher NLS, longer durations of electrical activity, CRF presence, and number of lightning flashes). More specifically, we speculate that higher NLS and higher probabilities of CRF generation are linked to the magma fragmentation, comminution, and collisional processes that happen within the conduit, whereas the probability and duration of lightning flashes are linked to plume processes.

To effectively integrate volcanic lightning into a monitoring context it is important to understand what different information radio frequency signals can tell us about the geophysical parameters of the source. We show that volcanic lightning is not singularly related to seismic or infrasound signals, but that the interactions between the seismic and infrasound signals are important for understanding the different volcanic processes at play. This work indicates the complexity of these relationships and that future work needs to be done to refine these models. The addition of more varied datasets – including other parameters such as located earthquakes and/or radar measurements of plume densities – from different volcanoes with different compositions and eruption types, will help determine what other parameters are correlated with parameters of electrical activity, as well as to improve error bounds.

Funding sources

Funding support for this work was made possible by National Science Foundation Grants AGS 1445704 and 1445703.

CRediT authorship contribution statement

Cassandra M. Smith: Conceptualization, Methodology, Formal analysis, Investigation, Data curation, Writing - original draft, Writing - review & editing, Visualization, Validation. **Glenn Thompson:** Methodology, Software, Resources, Data curation, Writing - review & editing. **Steven Reader:** Conceptualization, Methodology, Software, Writing - review & editing, Validation. **Sonja A. Behnke:** Conceptualization, Investigation, Resources, Writing - review & editing, Validation, Supervision, Funding acquisition. **Stephen R. McNutt:** Conceptualization, Investigation, Resources, Writing - review & editing, Supervision, Project administration, Funding acquisition. **Ron Thomas:** Software, Investigation, Validation. **Harald Edens:** Software, Investigation.

Declaration of competing interest

The authors declare that they have no known competing financial interests or personal relationships that could have appeared to influence the work reported in this paper.

Acknowledgements

The authors would like to thank Sylvain Charbonnier and the anonymous reviewers whose comments improved this manuscript. We would also like to thank Masato Iguchi, Daisuke Miki, and all of the

Sakurajima Volcano Observatory for their assistance during data collection.

Data availability

All data will be publicly available through the USF library digital collections at https://digital.lib.usf.edu/volcanic-lightning/.

Appendix A. Supplementary data

Supplementary data to this article can be found online at https://doi.org/10.1016/j.jvolgeores.2020.106996.

References

Arason, P., Bennett, A.J., Burgin, L.E., 2011. Charge mechanism of volcanic lightning revealed during the 2010 eruption of Eyjafjallajökull. J. Geophys. Res. Solid Earth 116 (12), 1–15. https://doi.org/10.1029/2011JB008651.

Behnke, S., Bruning, E., 2015. Changes to the turbulent kinematics of a volcanic plume inferred from lightning data. Geophys. Res. Lett. 42 (10), 4232–4239. https://doi.org/10.1002/2015GL064199.

Behnke, S.A., McNutt, S.R., 2014. Using lightning observations as a volcanic eruption monitoring tool. Bull. Volcanol. 76, 1–12. https://doi.org/10.1007/s00445-014-0847-1.

Behnke, S.A., Thomas, R.J., McNutt, S.R., Schneider, D.J., Krehbiel, P.R., Rison, W., Edens, H.E., 2013. Observations of volcanic lightning during the 2009 eruption of Redoubt Volcano. J. Volcanol. Geotherm. Res. 259, 214–234. https://doi.org/10.1016/j.jvolgeores.2011.12.010.

Behnke, S.A., Thomas, R.J., Edens, H.E., Krehbiel, P.R., Rison, W., 2014. The 2010 eruption of Eyjafjallajökull: Lightning and plume charge structure. J. Geophys. Res. Atmos. 119, 833–859. https://doi.org/10.1002/2013JD020781.

Behnke, S.A., Edens, H.E., Thomas, R.J., Smith, C.M., McNutt, S.R., Van Eaton, A.R., Cimarelli, C., Cigala, V., 2018. Investigating the origin of continual radio frequency impulses during explosive volcanic eruptions. J. Geophys. Res. Atmos. 123, 4157–4174. https://doi.org/10.1002/2017JD027990.

Cashman, K.V., Scheu, B., 2015. Magmatic fragmentation. In: Sigurdsson, H., Houghton, B., McNutt, S.R., Rymer, H., Stix, J. (Eds.), The Encyclopedia of Volcanoes. Academic Press, Cambridge, pp. 459–471 https://doi.org/10.1016/B978-0-12-385938-9.00025-0.

Cimarelli, C., Alatorre-Ibargüengoitia, M.A., Aizawa, K., Yokoo, A., Díaz-Marina, A., Iguchi, M., Dingwell, D.B., 2016. Multiparametric observation of volcanic lightning: Sakurajima Volcano, Japan. Geophys. Res. Lett. 43, 4221–4228. https://doi.org/10.1002/2015GL067445.

Clarke, A.B., Ongaro, T.E., Belousov, A., 2015. Vulcanian Eruptions. In: Sigurdsson, H., Houghton, B., McNutt, S.R., Rymer, H., Stix, J. (Eds.), The Encyclopedia of Volcanoes. Academic Press, Cambridge https://doi.org/10.1016/B978-0-12-385938-9.00028-6.

Fox, J., 2003. Effect displays in R for generalised linear models. J. Stat. Softw. 8, 1–27.

Fox, J., 2016. Applied Regression Analysis & Generalized Linear Models. Third Edit. SAGE.

Fox, J., Weisberg, S., 2011. An {R} Companion to Applied Regression. Second Edi. Sage, Thousand Oaks, CA.

Garcés, M., Iguchi, M., Ishihara, K., Morrissey, M., Sudo, Y., Tsutsui, T., 1999. Infrasonic precursors to a vulcanian eruption at Sakurajima volcano, Japan. Geophys. Res. Lett. 26, 2537. https://doi.org/10.1029/1998GL005327.

Gaudin, D., Cimarelli, C., 2019. The electrification of volcanic jets and controlling parameters: a laboratory study. Earth Planet. Sci. Lett. 513, 69–80. https://doi.org/10.1016/j.epsl.2019.02.024.

Gaudin, D., Cimarelli, C., Becker, V., Knüver, M., 2018. What controls the occurrence of lightning in volcanic ash plumes: A quantitative lab analysis. EGU General Assembly Conference Abstracts.

Hamlin, T.D., 2004. The New Mexico Tech Lightning Mapping Array. New Mexico Institute of Mining and Technology.

Hargie, K.A., Van Eaton, A.R., Mastin, L.G., Holzworth, R.H., Ewert, J.W., Pavolonis, M., 2019. Globally detected volcanic lightning and umbrella dynamics during the 2014 eruption of Kelud, Indonesia. J. Volcanol. Geotherm. Res. 382, 81–91.

Hoblitt, R.P., 1994. An experiment to detect and locate lightning associated with eruptions of Redoubt Volcano. J. Volcanol. Geotherm. Res. 62 (1–4), 499–517. https://doi.org/10.1016/0377-0273(94)90049-3.

Iguchi, M., Tanegyri, T., Ohta, Y., Ueki, S., Nakao, S., 2013. Characteristics of volcanic activity at Sakurajima volcano's Showa Crater during the period 2006 to 2011. Bull. Volcanol. Soc. Japan 58, 115–135. https://doi.org/10.18940/kazan.58.1_115.

Ishihara, K., 1985. Dynamical analysis of volcanic explosion. J. Geodyn. 3 (3–4), 327–349. https://doi.org/10.1016/0264-3707(85)90041-9.

James, M.R., Wilson, L., Lane, S.J., Gilbert, J.S., Mather, T.A., Harrison, R.G., Martin, R.S., 2008. Electrical charging of volcanic plumes. Space Sci. Rev. 137, 399–418. https://doi.org/10.1007/s11214-008-9362-z.

Johnson, J.B., Aster, R.C., 2005. Relative partitioning of acoustic and seismic energy during Strombolian eruptions. J. Volcanol. Geotherm. Res. 148, 334–354. https://doi.org/10.1016/j.jvolgeores.2005.05.002.

Johnson, J.B., Ripepe, M., 2011. Volcano infrasound: a review. J. Volcanol. Geotherm. Res. 206, 61–69. https://doi.org/10.1016/j.jvolgeores.2011.06.006.

Lumley, T., 2017. based on Fortran code by Alan Miller. Leaps: Regression Subset Selection.

Marchetti, E., Ripepe, M., Harris, a.J.L., Delle Donne, D., 2009. Tracing the differences between Vulcanian and Strombolian explosions using infrasonic and thermal radiation energy. Earth Planet. Sci. Lett. 279 (3–4), 273–281. https://doi.org/10.1016/j.epsl.2009.01.004.

McNutt, S.R., Williams, E.R., 2010. Volcanic lightning: Global observations and constraints on source mechanisms. Bull. Volcanol. 72, 1153–1167. https://doi.org/10.1007/s00445-010-0393-4.

McNutt, S.R., Thompson, G., West, M.E., Fee, D., Stihler, S., Clark, E., 2013. Local seismic and infrasound observations of the 2009 explosive eruptions of Redoubt Volcano, Alaska. J. Volcanol. Geotherm. Res. 259, 63–76. https://doi.org/10.1016/j.jvolgeores.2013.03.016.

McNutt, S.R., Thompson, G., Johnson, J., Angelis, S. De, 2015. Seismic and Infrasonic monitoring. In: Sigurdsson, H., Houghton, B., McNutt, S.R., Rymer, H., Stix, J. (Eds.), The Encyclopedia of Volcanoes. Academic Press, Cambridge https://doi.org/10.1016/B978-0-12-385938-9.00063-8.

Méndez Harper, J., Dufek, J., 2016. The effects of dynamics on the triboelectrification of volcanic ash. J. Geophys. Res. Atmos., 8209–8228 https://doi.org/10.1002/2015JD024663.

Méndez Harper, J.S., Cimarelli, C., Dufek, J., Gaudin, D., Thomas, R.J., 2018. Inferring compressible fluid dynamics from vent discharges during volcanic eruptions. Geophys. Res. Lett. 45, 7226–7235. https://doi.org/10.1029/2018GL078286.

Morrissey, M.M., Chouet, B.A., 2010. Burst conditions of explosive volcanic eruptions recorded on microbarographs burst conditions of explosive volcanic eruptions recorded on microbarographs. World 1290, 1–5. https://doi.org/10.1126/science.275.5304.1290.

Morrissey, M., Garces, M., Ishihara, K., Iguchi, M., 2008. Analysis of infrasonic and seismic events related to the 1998 Vulcanian eruption at Sakurajima. J. Volcanol. Geotherm. Res. 175, 315–324. https://doi.org/10.1016/j.jvolgeores.2008.03.008.

Nicoll, K., Airey, M., Cimarelli, C., Bennett, A., Harrison, G., Gaudin, D., ... Marlton, G., 2019. First in situ observations of gaseous volcanic plume electrification geophysical research letters. Geophys. Res. Lett. https://doi.org/10.1029/2019GL082211.

Prata, A.T., Folch, A., Prata, A.J., Biondi, R., Brenot, H., Cimarelli, C., Corradini, S., 2020. Anak Krakatau triggers volcanic freezer in the upper troposphere. Sci. Rep., 1–13 https://doi.org/10.1038/s41598-020-60465-w.

R Core Team, 2017. R: a language and environment for statistical computing. R Foundation for Statistical Computing, Vienna, Austriahttp://www.R-project.org/.

Rakov, V.A., 2013. Electromagnetic Methods of Lightning Detection. Surv. Geophys. 34, 731–753. https://doi.org/10.1007/s10712-013-9251-1.

Rison, W., Thomas, R.J., Krehbiel, P.R., Hamlin, T., Harlin, J., 1999. A GPS-based three-dimensional lightning mapping system: initial observations in Central New Mexico. Geophys. Res. Lett. 26, 3573–3576. https://doi.org/10.1016/j.jval.2016.03.1245.

Sarkar, D., 2008. Lattice: Multivariate Data Visualization. R. Springer, New York.

Shevtsov, B.M., Firstov, P.P., Cherneva, N.V., Holzworth, R.H., Akbashev, R.R., 2016. Lightning and electrical activity during the Shiveluch volcano eruption on 16 November 2014. Nat. Hazards Earth Syst. Sci. 16 (3), 871–874. https://doi.org/10.5194/nhess-16-871-2016.

Smith, C.M., Van Eaton, A.R., Charbonnier, S., McNutt, S.R., Behnke, S.A., Thomas, R.J., Edens, H.E., Thompson, G., 2018. Correlating the electrification of volcanic plumes with ashfall textures at Sakurajima Volcano, Japan. Earth Planet. Sci. Lett. 492, 47–58. https://doi.org/10.1016/j.epsl.2018.03.052.

Stern, S., Cimarelli, C., Gaudin, D., Scheu, B., Dingwell, D.B., 2019. Electrification of experimental volcanic jets with varying water content and. Temperature Geophysical Research Letters (1), 1–10 https://doi.org/10.1029/2019GL084678.

Tameguri, T., Iguchi, M., Ishihara, K., 2002. Mechanism of explosive eruptions from moment tensor analyses of explosive earthquakes at Sakurajima volcano, Japan. Bull. Volcanol. Soc. Japan 47, 197–215.

Thomas, R.J., Krehbiel, P.R., Rison, W., Harlin, J., Hamlin, T., Campbell, N., 2003. The LMA flash algorithm. Proc. 12th Int. Conf. On Atmospheric Electricity, International Commission on Atmospheric Electricity Versailles, France, pp. 655–656.

Thomas, R.J., Krehbiel, P.R., Rison, W., Hunyady, S.J., Winn, W.P., Hamlin, T., Harlin, J., 2004. Accuracy of the lightning mapping array. J. Geophys. Res. D Atmos. 109, 1–34. https://doi.org/10.1029/2004JD004549.

Thomas, R.J., Krehbiel, P.R., Rison, W., Edens, H.E., Aulich, G.D., Winn, W.P., McNutt, S.R., Tytgat, G., Clark, E., 2007. Electrical activity during the 2006 Mount St. Augustine volcanic eruptions. Science (80) 315, 1097.

Thomas, R.J., McNutt, S.R., Krehbiel, P.R., Rison, W., Aulich, G., Edens, H.E., Tytgat, G., Clark, E., 2010. Lightning and electrical activity during the 2006 Eruption of Augustine volcano. In: Power, J.A., Coombs, M.L., Freymueller, J.T. (Eds.), The 2006 Eruption of Augustine Volcano, Alaska. U.S. Geological Survey Professional Paper, pp. 579–608.

Uhira, K., Takeo, M., 1994. The source of explosive eruptions of Sakurajima volcano, Japan. J. Geophys. Res. 99, 17775–17789. https://doi.org/10.1029/94JB00990.

Van Eaton, A.R., Amigo, A., Bertin, D., Mastin, L.G., Giacosa, R.E., Gonzalez, J., Valderrama, O., Fontijn, K., Behnke, S.A., 2016. Volcanic lightning and plume behavior reveal evolving hazards during the April 2015 eruption of Calbuco volcano, Chile. Geophys. Res. Lett., 3563–3571 https://doi.org/10.1002/2016GL068076.

Van Eaton, A.R., Schneider, D.J., Smith, C.M., Haney, M.M., Lyons, J.J., Said, R., Mastin, L.G., 2020. Did ice-charging generate volcanic lightning during the 2016–2017 eruption of Bogoslof volcano, Alaska? Bull. Volcanol. 82 (3), 24. https://doi.org/10.1007/s00445-019-1350-5.

Woodhouse, M.J., Behnke, S.A., 2014. Charge structure in volcanic plumes: a comparison of plume properties predicted by an integral plume model to observations of volcanic lightning during the 2010 eruption of Eyjafjallajökull, Iceland. Bull. Volcanol. 76, 1–21. https://doi.org/10.1007/s00445-014-0828-4.

Yokoo, A., Tameguri, T., Iguchi, M., 2009. Swelling of a lava plug associated with a Vulcanian eruption at Sakurajima Volcano, Japan, as revealed by infrasound record: Case study of the eruption on January 2, 2007. Bull. Volcanol. 71, 619–630. https://doi.org/10.1007/s00445-008-0247-5.

Yokoo, a., Suzuki, Y.J., Iguchi, M., 2014. Dual infrasound sources from a vulcanian eruption of Sakurajima volcano inferred from cross-array observation. Seismol. Res. Lett. 85, 1212–1222. https://doi.org/10.1785/0220140047.